# Electromagnetic Optimization of FRC-Based Pulsed Plasma Thrusters


**IEPC-2013-376**

*Presented at the 33rd International Electric Propulsion Conference,*
*The George Washington University • Washington, D.C. • USA*
*October 6 – 10, 2013*



Jamie Waldock[1]
*University of Washington, Seattle, WA, 98105, United States*

Dr. David Kirtley[2] and Dr. John Slough[3]
*MSNW LLC., Redmond, WA, 98052, United States*



**Abstract:** **The ElectroMagnetic Plasmoid Thruster (EMPT) at MSNW LLC. is a 1 kW, electrodeless pulsed plasma thruster that generates and accelerates a Field Reversed Configuration (FRC) to produce thrust. Two key components of the thruster are the RF antennas that generate a Rotating Magnetic Field (RMF), which produces azimuthal plasma currents and form the FRC, and the flux conserving rings, which provide radial pressure balance to the FRC. Magnetic coupling between these two components, as well as the overall plasma loading efficiency of the thruster are affected by the material and geometry of each component, which determine how the RMF is shaped. In this study an in-air, to scale version of EMPT was created and used to test various RF antenna and flux conserver combinations on dummy loads. Measurements of the Q loading factors and magnitudes of the internal radial magnetic field were used to evaluate the combinations and identify general trends. Results of testing yielded several important conclusions about the materials and geometries that lead to better thruster performance. Firstly, aluminum flux rings are less permeable to the RMF and lead to greater resistive coupling between the antennas than do copper flux rings. Likewise, flux ring geometries with greater surface coverage lead to more shielding. Of all antennas tested, the lapped geometries produced greater internal, radial magnetic fields for the same energy input and dissipated more energy per cycle to the load. The most recent version of the EMPT thruster utilized large aluminum structural plates and an RF antenna with doubled geometry. Based on the results of this study, the EMPT thruster has been redesigned accordingly.**


## Nomenclature

| | | |
|---|---|---|
| $j_\theta$ | = | azimuthal current |
| $e$ | = | elementary charge |
| $j_\theta$ | = | azimuthal current |
| $n_e$ | = | electron density |
| $\omega$ | = | angular frequency |
| $r$ | = | radial position |
| $F_z$ | = | axial force |
| $B$ | = | magnetic field magnitude |
| $B_{r\ bias}$ | = | radial component of bias field |
| $V$ | = | voltage |


[1] Research Intern, jdock@u.washington.edu
[2] Propulsion Research Scientist, dkirtley@msnwllc.com
[3] President and Director of Research, sloughj@msnwllc.com

| | | |
|---|---|---|
| $R$ | = | resistance |
| $L$ | = | inductance |
| $M$ | = | magnetic coupling factor between antennas |
| $I$ | = | current |
| $I_1$ | = | current in antenna A |
| $I_2$ | = | current in antenna B |
| $t$ | = | time |
| $f$ | = | frequency |
| $C$ | = | capacitance |
| $E$ | = | energy |
| $N$ | = | number of loops |
| $\Phi$ | = | magnetic flux |
| $A$ | = | area |
| $R_{int}$ | = | analog integrator circuit resistor value |
| $C_{int}$ | = | analog integrator circuit capacitor value |
| $\delta$ | = | classical skin depth |
| $\rho$ | = | resistivity of material |
| $\mu$ | = | absolute magnetic permeability of material |
| $Q$ | = | q factor |
| $B_R$ | = | internal radial magnetic field component |
| $B_{R, norm}$ | = | normalized internal radial magnetic field component |
| $V_2$ | = | voltage at 2 cycles after discharge, 2nd peak |
| $V3$ | = | voltage at 3 cycles after discharge, 3rd peak |

## I. Introduction

THE Electromagnetic Plasmoid Thruster (EMPT), currently undergoing testing at MSNW LLC., is a 1 kW, electrodeless pulsed plasma thruster and power processing system that offers a decrease in system mass and superior thrust efficiency over traditional thrusters in the same power class, resulting in high specific power (>700 W/kg) and high thrust-to-power[1]. It can be operated over a range of 200-2000 W. And due to the magnetic self-containment of the FRC, EMPT's lifetime is also not limited by electrode or wall erosion, typical problems for other thruster types. A recent version of EMPT is shown in Fig. 1 with its components labeled. EMPT has been tested using a wide range of fuels including xenon, argon, and Hydrazine simulant, while its larger counterpart the Electrodeless Lorentz Force thruster (ELF)[2] has also been operated using nitrogen, oxygen, air, water, and Martian atmosphere[3]. Optimizing EMPT to operate on in situ gases–more molecularly inefficient, but abundant–will allow for reductions in propellant mass and overall cost of asteroid or planetary sample return missions, as well as applications where low or eccentric orbits must be maintained. Other applications of EMPT include satellite station keeping, LEO-to-GEO transfers, and deep space missions[1]. This ability to be optimized for a wide range of mission types makes EMPT ideal for defensive, scientific, and commercial applications.

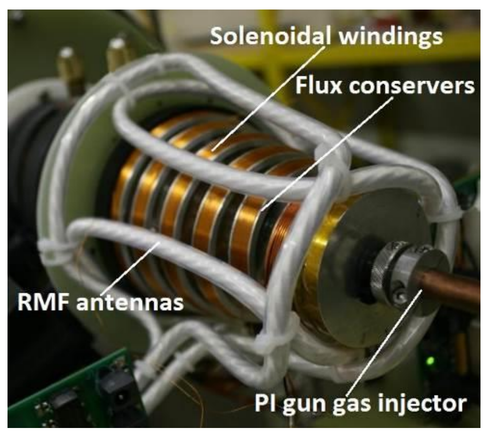


**Figure 1. The EMPT Thruster.**
*An older design with aluminum flux rings beneath copper bias coils and a doubled 1-turn Litz wire RMF antenna.*

The presented study was conducted to investigate the effects of varying the geometries and materials of the RMF antenna and flux conserver components, crucial to its operation. Specifically, resistive coupling between antennas or between the antennas and flux conserving rings is a loss mechanism that should be minimized, while other coupling between the antennas and plasma load is to be maximized to increase thrust. RMF antenna geometries examined in the study were saddle antennas in doubled and lapped configurations with 1 or 2 turn loops, connected either in parallel or series. The materials composing the antennas were either AWG 3, type 5 copper Litz or flattened 3/8 inch solid copper tubing. The flux conserver rings tested lay flush to the cone surface and had surface coverage opacities of 25, 50, or 90 percent; they were composed of copper or aluminum of various widths and numbers of rings.

Magnetic field probes monitored axial and radial magnetic fields internal and external to the cone, while voltage probes monitored the voltage on the capacitor banks. During testing, the capacitance and supply voltage of the LC oscillator circuits were adjusted to maintain a frequency of 300 kHz and maintain the same stored electrical energy for all component combinations. Using these diagnostics, antenna and stray inductance, internal and external magnetic field strength, and overall circuit Q factor could be determined and used to compare the different geometric and material combinations.

### A. FRC Formation

The process of producing thrust by forming an FRC plasmoid[4] begins with triggering coils wrapped around the conical nozzle that establish an axial steady state bias field. Shortly after gas is injected through a pre-ionization electrode, providing a very small seed plasma. The RMF antennas, placed orthogonal from one other and operated 90 degrees out of phase, then drive an oscillating current[5] that produce a steady Rotating Magnetic Field[6]. This field fully ionizes the gas and produces a strong azimuthal current (up to 20 KA). This current[7] then acts to reverse the field within the plasma, creating a magnetically isolated, self-contained FRC plasmoid[4]. Currents are induced within the flux preserving rings around the cone, which in turn provide radial pressure balance to the plasmoid. The FRC is then expelled at high velocity via the Lorentz force and thermal expansion to produce thrust. The full formation and ejection process, illustrated in Fig. 2, takes less than 20 µs. In tests, EMPT has been steady state operated over a range of 1-3 kHz with discharges of 0.5-1 J and has demonstrated over 1E9 continuous plasma discharges[1]. An example xenon plasma discharge is also shown in Fig. 2c. The relationship between azimuthal plasma current, RF angular frequency, bias field, and Lorentz force is shown in Eqn. 1 and 2.

$$j_\theta(r) = e n_e \omega r \tag{1}$$

$$F_z = j_\theta \times B_{rbias} \tag{2}$$

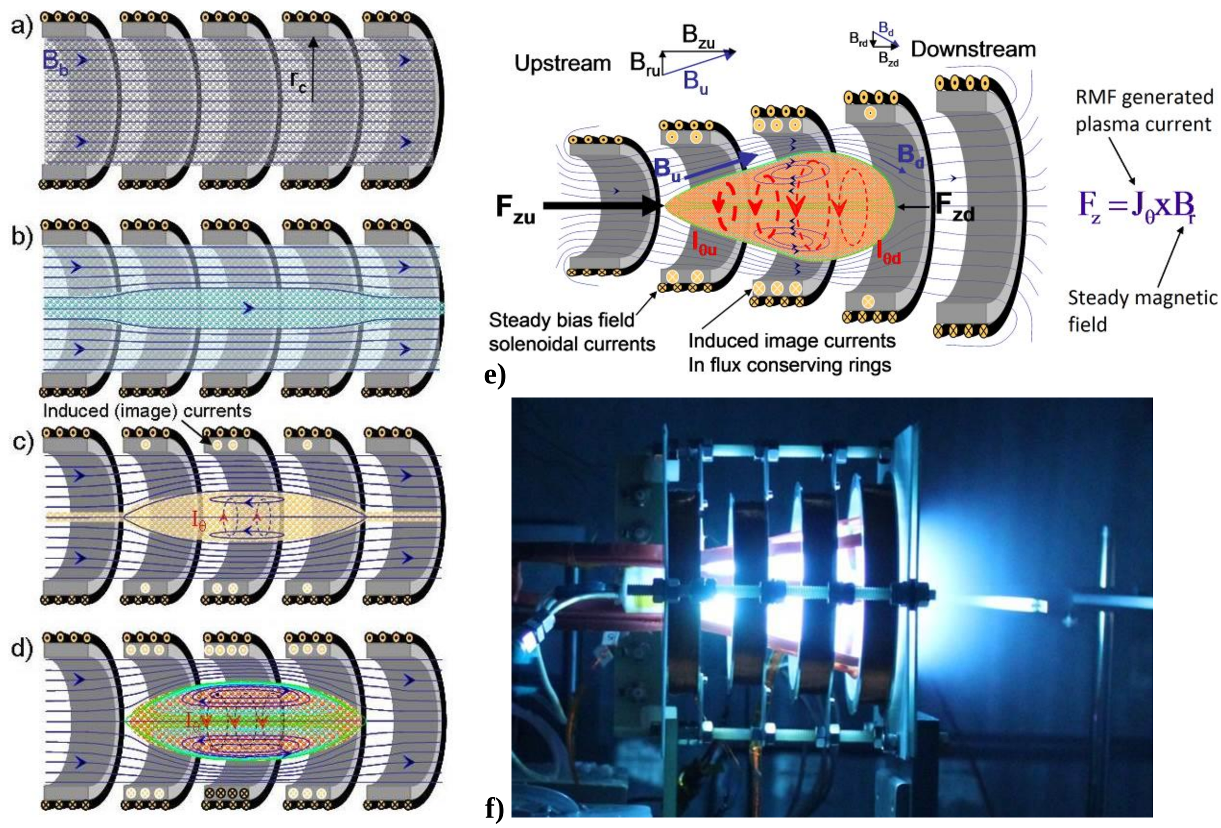


**Figure 2. FRC formation.**
*a) steady bias field, b) gas injection and ionization by RMF, c) magnetic field reversal by azimuthal current, d) FRC plasmoid formation, e) conical bias field, thermal expansion, and Lorentz force ejection, and f) xenon operation of newly redesigned EMPT.*

## B. RF Antenna Material and Geometry

To understand how manipulating the geometry or material of the RF antennas affects how the thruster performs, the physics behind how it produces a Rotating Magnetic Field must be explained. The saddle RMF antennas used by EMPT, shown in Fig. 3, are not unique in their ability to produce a rotating magnetic field, as spiral antennas and other such geometries can do the same. Saddle antennas, however, are optimal for RMF and electromagnetic plasmas, as is explained more fully in the references[1]. Each saddle RMF antenna is composed of two loops placed across from one another, connected in parallel or in series. The full RMF antenna is constructed from two RF antennas placed orthogonal to one another around the cone. When the antennas are triggered they oscillate at the LC circuit frequency; triggering them 90 degrees out of phase from one another produces a Rotating Magnetic Field. In the doubled RMF geometry one RF antenna is constructed of narrower loops than the other in order to fully lie inside it and create a symmetric geometry as shown in Fig. 4a, where the bottom edges of the antennas are shown. In the lapped RMF geometry all loops are of the same size, with the far edge of each lapped over the next one to produce a net helical geometry as shown in Fig. 4b. Finally, whether connected in parallel or series, the direction of the current through the loop pairs must be such that they produce a magnetic field in the same direction. In Fig. 4c an example of this is shown, where the current in the vertical leg of each loop matches that of the neighboring leg on the other loop.

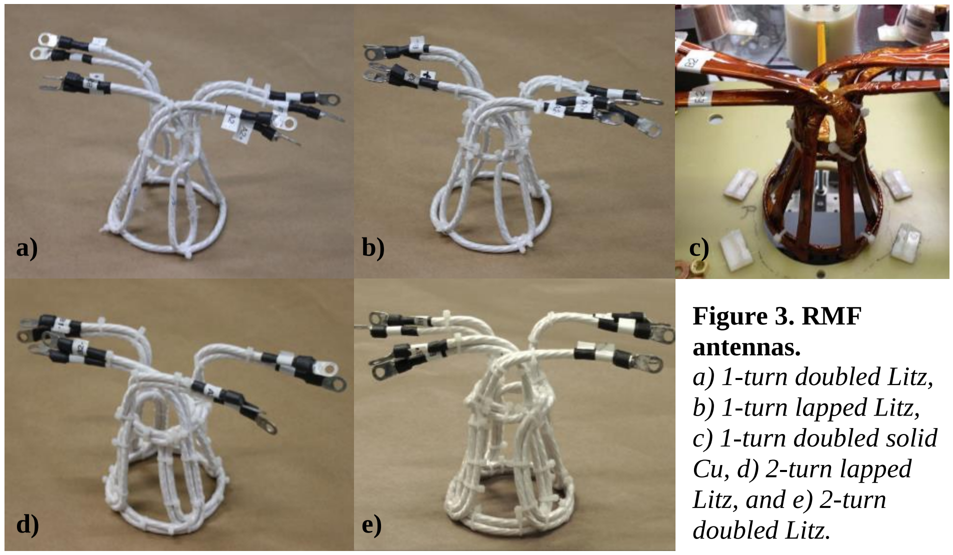


**Figure 3. RMF antennas.**
*a) 1-turn doubled Litz, b) 1-turn lapped Litz, c) 1-turn doubled solid Cu, d) 2-turn lapped Litz, and e) 2-turn doubled Litz.*

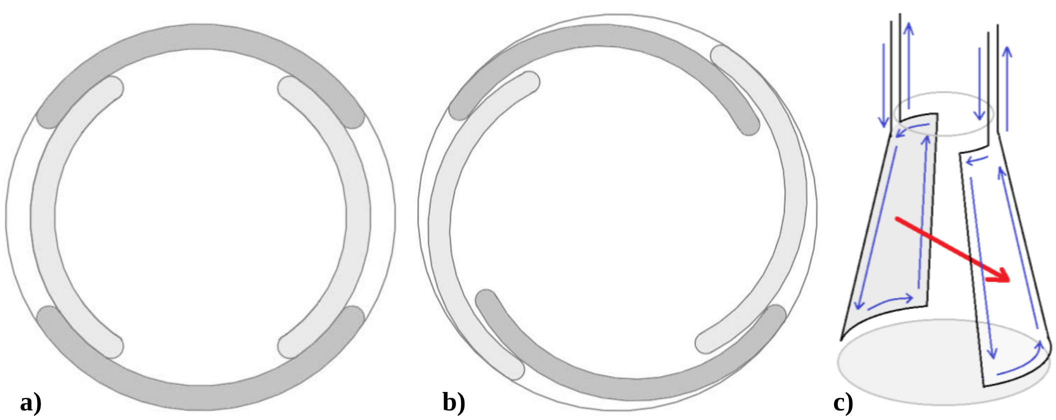


**Figure 4. RMF antenna geometries as viewed from below and current flow within them.**
*a) doubled, b) lapped, and c) aligned current in ajacent branches.*

The symmetry of the doubled antenna is thought to produce an RMF that remains centered, but with a fluctuating magnitude because of the difference in sizes of the antenna pairs. Conversely, the lapped antenna is thought to maintain an RMF with a constant magnitude, but with a center that rotates slightly about the middle of the cone because of the angled lapping of loops, resulting in a net helical field. As for the antenna material, using Litz wire mitigates adverse skin depth effects, but introduces complex magnetic fields within the braid. Moreover, the Litz wire has a low critical temperature relative to the rest of the thruster system, as well as a flexibility that makes maintaining a constant antenna shape challenging. Using solid copper eliminates the complex fields, but adds system mass and difficulty of manufacturing. While solid copper leads to higher heating losses, its much higher critical temperature allows it to withstand these higher temperatures. The final shape of the RMF determines how well the azimuthal plasma currents are induced, which in turn determines the overall performance of the thruster. The RF antenna pairs are meant to fully couple magnetically to the plasma to achieve high thruster efficiency, but will couple resistively to one another to some degree and result in system performance and energy loss; an antenna geometry that mitigates this resistive coupling is desired.

### C. Flux Conserver Ring Material and Geometry

The equally crucial flux conserving ring components function by carrying induced currents that provide radial magnetic pressure balance to the FRC, which would otherwise expand onto the thruster walls. Therefore, these rings do remove some small amount of energy from the system through magnetic coupling with the plasma and antennas, which is to be expected, but can remove larger amounts of energy if they become too resistively coupled to the RF antennas. And because the flux conservers lie within the RF antennas, they also shield the center of the cone to some degree, thus reducing the effectiveness of the RMF to penetrate and produce strong azimuthal plasma currents. By varying the width and number of rings, a surface coverage, or opacity, may be achieved that reduces coupling between the rings and RF antennas, as well as allows for greater RMF permeability; these variations are shown in Fig. 5. The choice of material for the flux conservers will mean a certain skin depth that affects the amount of current that can be induced within them. Modifying the thickness of the rings can help optimize these skin depth effects. The final phenomenon to take into consideration is how the presence of the flux conservers can lead to increased coupling between the antenna pairs. Because of this multitude of complex interactions between the antennas, flux conservers, and plasma, it is difficult to predict which combination of RF antennas and flux conserving rings will reduce the ill effects mentioned and lead to improved thruster performance. The equation describing the voltage within one half of the RMF antenna, as affected by magnetic coupling with the other antenna half, is shown below in Eqn. 3.

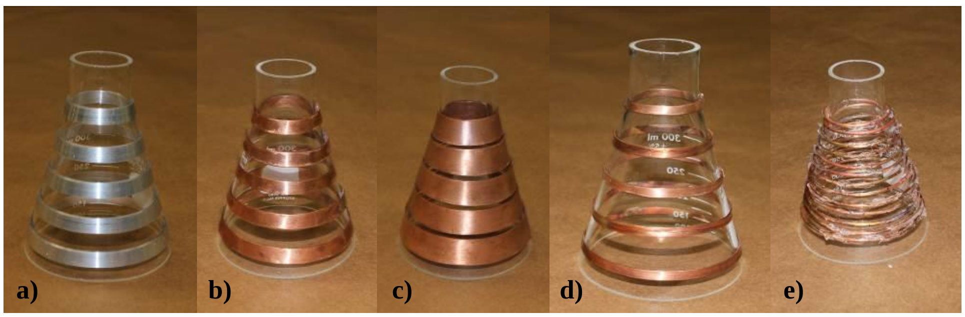

**Figure 5. Flux conserving rings tested.**
*a) five 50% coverage aluminum, b) five 50% coverage copper, c) five 90% coverage copper, d) five 25% coverage copper, and e) 13 50% coverage copper.*

$$V_1 = R_1 I_1 + L_1 \frac{dI_1}{dt} + M \frac{dI_2}{dt} \tag{3}$$

## II. Experimental Method

The goal of the study was to identify the combination of flux conserving rings and RMF antenna material and geometry that maximized energy dissipation to the plasma. These optimization tests were carried out in air on a lab bench setup where an RMF antenna was mounted on top of a G10 fiberglass table and connected to the oscillator circuits via wide, copper stripline. A hole in the table allowed for a glass thruster cone, of the same dimensions as EMPT's nozzle, to fit vertically through the hole and be held in place by a supporting plate from below. This allowed for the RF antenna to remain undisturbed for the entire duration of a series of tests, while the glass cone, flux conserving rings, plasma simulator dummy loads, and internal magnetic probe could be removed through the bottom. The internal and external magnetic probes were mounted to long plastic rods and were held in place with clamps. Wall warts supplied DC power to the IGBT circuit boards. The inductors and capacitance banks were elevated on the G10 table, while the diodes were grounded underneath to the lab bench. The voltage on the capacitance banks were monitored by voltage probes connected to the oscilloscope. A picture of the entire experimental setup is shown in Fig. 6.

An oscillator circuit attached to each half of the RF antenna, one being labeled "A" and the other "B" for the entire duration of tests, was made up of a large coil inductor of 500 uH, a 1200 V diode, a capacitance bank, a Semikron IGBT switch rated to 1700 V, and a linear DC power supply. The diodes act to keep charge on the capacitors while the large coil inductors store up energy during the on switch phase that is then dumped into the capacitors during the off switch phase, thus allowing for the voltage across the capacitors to reach a much higher value than that of the supply. The two oscillator circuits' switches were fiberoptically triggered by a single pulse generator which produced two 250 μs pulses, 500 μs apart, ensuring that the second trigger fully charged the capacitance banks to a voltage far above that of the supply. The oscillator circuit design is shown in Fig.7 for the case in which a 1-turn, doubled Litz antenna is being tested.

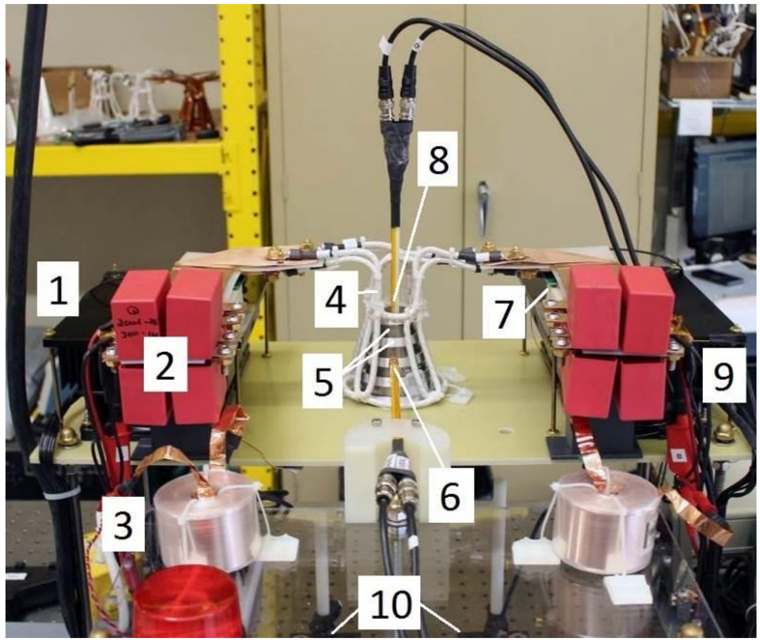

**Figure 6. Experimental test setup.**
*1) heat sink and cooling fans for IGBT switches, 2) capacitance banks, 3) inductor coils, 4) RMF antenna, 5) glass support cone and flux conserving rings, 6) external magnetic probe, 7) IGBT switch, 8) internal magnetic probe, 9) capacitor voltage probes, and 10) diodes.*

As was mentioned in the Introduction, the capacitance value of the circuits was adjusted throughout the experiment, depending on the inductance of the RF antenna being tested in order to fix the oscillation frequency of the circuit at 300 kHz for all tests, according to Eqn. 4. Using an LCR meter the inductance and resistance of each RF antenna was measured over a range of 5 to 400 kHz. The supply voltage of the first test was set arbitrarily to 70 V, resulting in 0.158 J within the system. This energy was held constant throughout the tests by varying the supply voltage and capacitance of the circuits according to Eqn. 5. Due to added inductance from the circuits, coupling between antennas, low resolution on the oscilloscope, and a limited size of capacitor, a circuit with a frequency of exactly 300 kHz and an energy of 0.158 J was not always obtained. To account for this, results were later normalized for comparison purposes. The inductances of all antennas tested at 300 kHz are shown in the Appendix in Table A.

$$\omega = 2\pi \ f = \frac{1}{\sqrt{LC}} \tag{4}$$

$$E_{const} = \frac{1}{2} C V^2 \tag{5}$$

The magnetic probes were constructed by wrapping copper wire on a square, plastic rod to create two coils oriented perpendicularly to one another. Each probe loop was connected to an RC integrator circuit to produce a voltage signal proportional to the magnetic field component being measured. The area and number of windings of the loops were chosen to ensure resolution of the magnetic field strength expected and by the resistance and capacitance values of the integrator circuit. Equations 6 and 7 govern these relations. The resistor and capacitor values chosen were 500 Ω and 10 uF, respectively, to resolve 1 to 500 Gauss into a 5 V signal. For reference, the largest field produced during the experiment was 354 G, while the smallest was 11 G. Errors in the probes' accuracy was estimated to be 10%, but normalization allows meaningful comparisons to be drawn between tests.

$$V = -N \frac{d\phi_B}{dt} = -N \frac{dB}{dt} A \tag{6}$$

$$B = \frac{-R_{\text{int}} C_{\text{int}}}{NA} V_{cap} \tag{7}$$

To construct the flux conserving rings to be tested, aluminum and copper skin depths were calculated for the desired circuit frequency of 300 kHz using Eqn. 8. Knowing the geometry of the thruster cone, the width of each ring needed to achieve surface coverages of 25%, 50%, and 90% for differing numbers of rings could be calculated. The aluminum flux rings were machined out of a solid aluminum cylinder, while the copper rings were made from arcs cut out of copper plate soldered together. The final dimensions of the different flux ring sets tested are shown in the Appendix in Table B.

$$\delta = \sqrt{\frac{2\rho}{\omega\mu}} \tag{8}$$

The copper Litz RF antennas were created by wrapping AWG 3 type 5 copper Litz on wooden jig forms. The raw ends of the loop leads were solder dipped to ensure even current distribution and then connected to ring terminals. One antenna half was labeled “A”, while the other was labeled “B”, to be connected to the correspondingly labeled oscillator circuits for all tests. The antennas are shown in Fig. 3. The solid copper antenna was formed by flattening 3/8ths inch copper tubing and then bending it into the same conical loops as the Litz antennas, either the doubled or lapped configurations. This antenna is shown in Fig. 3c.

All antennas were tested with and without steel dummy loads, with and without flux rings, and all the combinations thereof, with a triggering phase shift of 0 or 90 degrees; the zero phase shift, where the antenna halves fire together, produces a simple oscillating magnetic field (OMF), while the 90 degree phase shift produces a Rotating Magnetic Field (RMF). The OMF cases simply served as a baseline for comparison. To determine the delay time to create the 90 degree phase shift, a test with no dummy loads or flux rings was performed to determine the actual frequency of the circuit. A quarter period of that oscillation was then used as the delay time, which had to be recalculated for each antenna tested. Finally, before testing could begin, the stray inductance (mostly due to stripline connections and the bends of the lead portions of the antennas) of each RF antenna half was adjusted so that both circuits oscillated with the same frequency and were as little coupled together as possible – i.e. one antenna should not absorb the energy of the other, rather they should oscillate down to zero voltage within the same amount of time. Coupling between antenna halves was expected to be worst when the aluminum flux conserver rings were present due to a larger skin depth, so in general these were present when adding stray inductance to decouple the antennas. These rings were then removed for subsequent test cases.

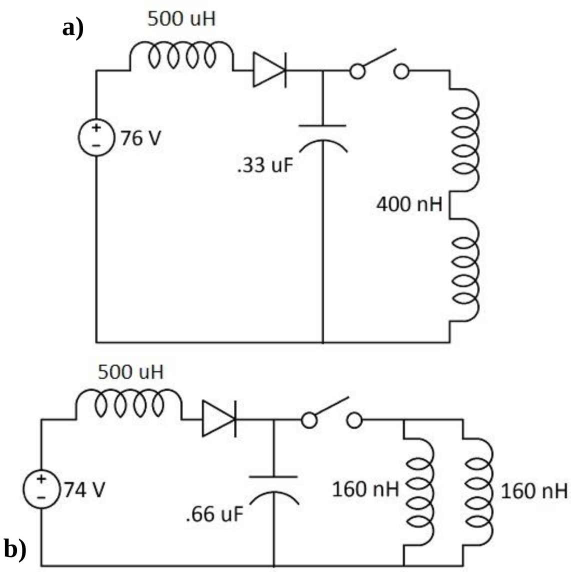


**Figure 7. Circuit diagram for the 1-turn doubled Litz RF antenna wired in a) series or b) parallel.**

## III. Results

To illustrate typical results, the capacitor voltage probes and internal radial magnetic probe signals for two tests of the 1-turn lapped Litz antenna connected in series are shown in Fig. 8 and 9. These cases illustrate that the highest internal, radial magnetic field is produced when flux rings and dummy loads are not present, which is to be expected since they act to absorb or shield the magnetic field from the center of the cone. For this same reason, the decay rate is also the longest in these cases. The 90 degree delay between antennas in the RMF case can be seen to cause the cumulative magnetic field produced to have a smaller first peak that grows when the second antenna is triggered.

Because of this, the maximum magnetic field magnitude never reaches that of the maximum value of the OMF case; OMF has total constructive interference, while RMF does not.

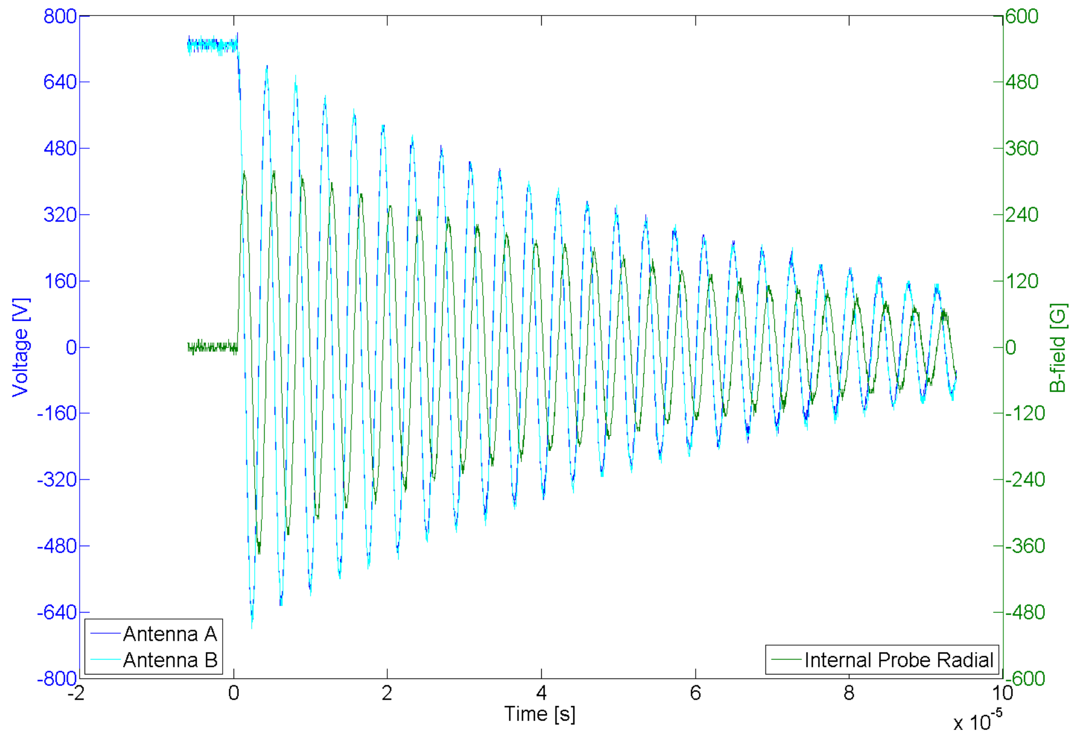


**Figure 8. OMF voltage and magnetic signals for 1-turn lapped Litz antenna connected in series with no flux conserving rings and no load.**

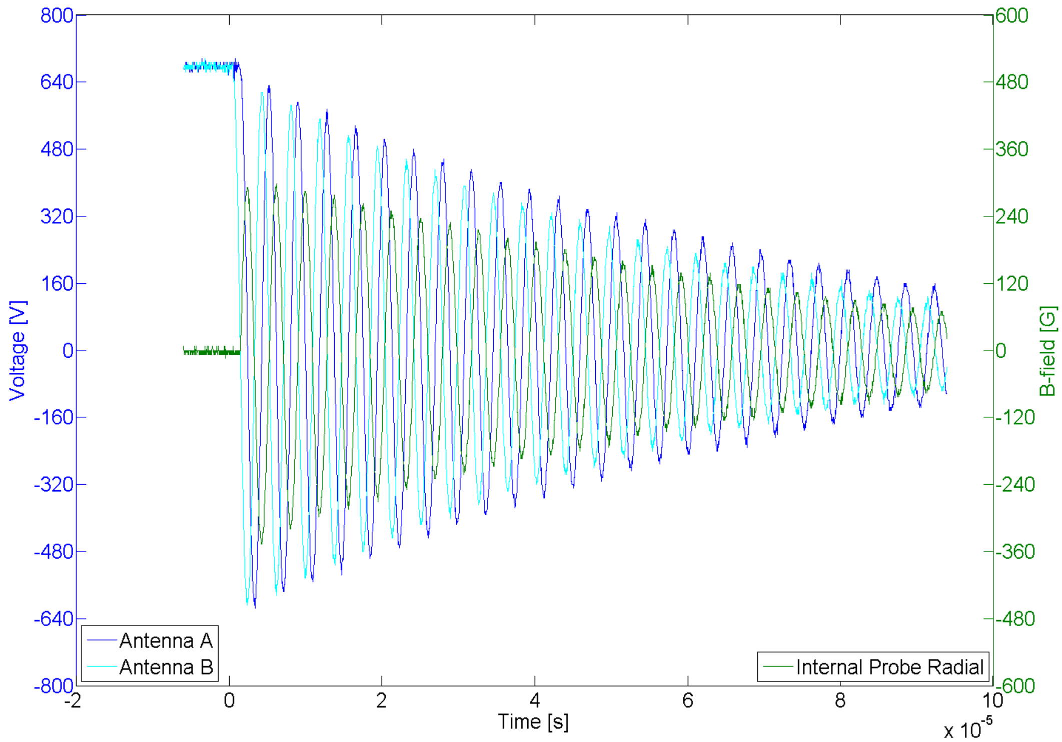


**Figure 9. RMF voltage and magnetic signals for 1-turn lapped Litz antenna connected in aeries with no flux conserving rings and no load.**

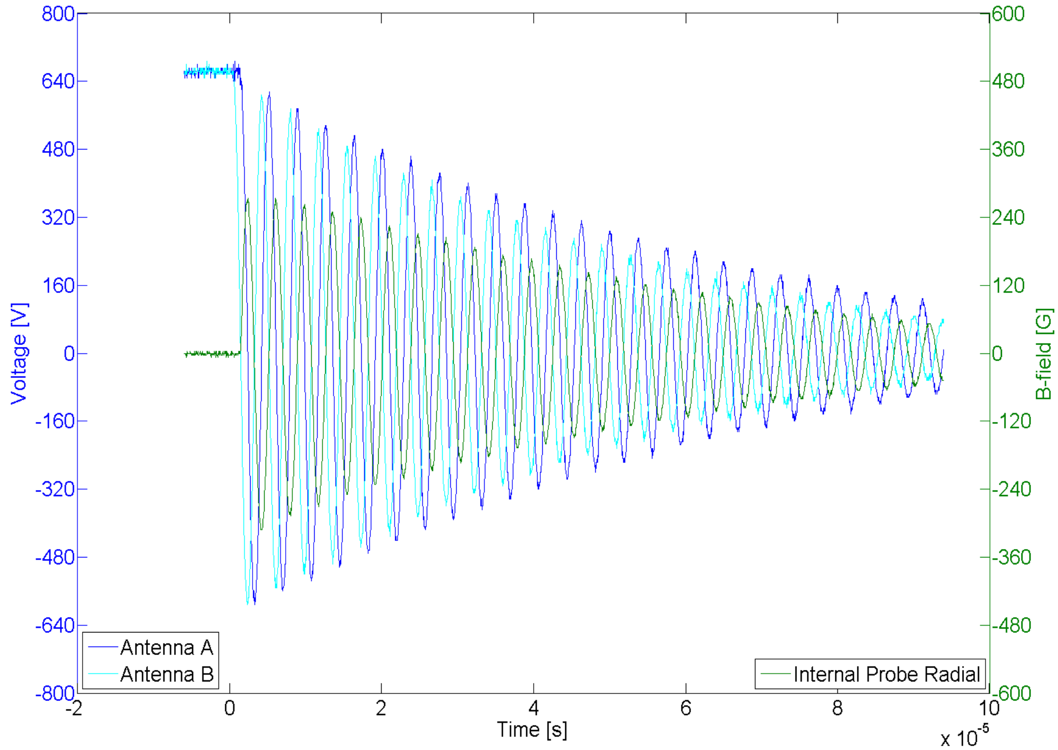


**Figure 10. 1-turn lapped Litz antenna connected in series with 5 Cu 50% flux rings.**

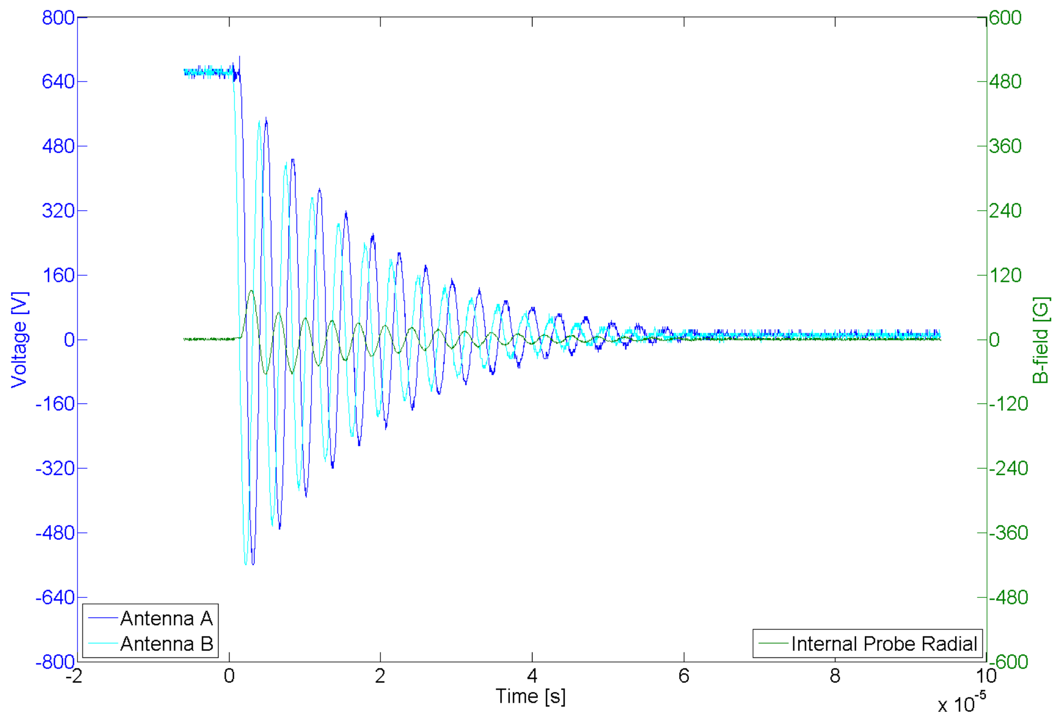


**Figure 11. 1-turn lapped Litz antenna connected in series with 5 Cu 50% flux rings and steel dummy load.**

When five copper flux rings with a total 50% opacity are added to the RMF operated setup to form a third test case, shown in Fig 10, the voltage signals decay faster and the internal magnetic field is reduced. When the steel dummy load is added to this in the fourth case, shown in Fig. 11, the antennas decay the fastest and the internal magnetic field is smallest, again because of the increased coupling and shielding. The coupling between antennas A and B, as seen by difference in voltage amplitude near the end of recording, changes somewhat when the rings and load are added; specifically, antenna A, the one being fired second, is being loaded with energy by antenna B. As was mentioned in the methods section, stray inductance was adjusted before testing to attempt to limit this from occurring, but could not always be avoided due to the imperfect nature of constructing the antennas and small differences between component values in circuits A and B.

Two of the most important outcomes of each test were the magnitude of the internal radial magnetic field component and the overall circuit Q factor. The radial magnetic field strength determines the strength of the azimuthal plasma current induced, and thus the rate of ionization and strength of the Lorentz force expelling the FRC. The Q factor, a ratio between energy stored and energy dissipated per cycle, measures how damped the system is, or in other words how much of the system's energy is dissipated per cycle by being absorbed by the load and flux rings through coupling. In Eqn. 9 Q factor is calculated using the magnetic field strength at the 2nd and 3rd peaks in the LC circuit's voltage oscillation.

$$Q = 2\pi \frac{E_{st}}{E_{disp}} = 2\pi \frac{V_2^2}{V_2^2 - V_1^2} \tag{9}$$

**Table 1. Results for 1-turn lapped Litz antenna connected in series for four standard cases.**

| Case | $Q_{avg}$ | $B_{R,\,norm}$ (G) |
|---|---|---|
| OMF only | 67±25% | 0.93 |
| RMF only | 62±24% | 0.82 |
| RMF, 5 Cu 50% flux rings | 65±14% | 0.79 |
| RMF, 5 Cu 50% flux rings with steel load | 19±5% | 0.15 |

Table 1 shows the Q factors, averaged between antenna circuits A and B for the four cases already presented and maximum internal radial magnetic field strength, normalized across all tests. The data reveals a decrease in Q as flux conserving rings and loads are added, indicating coupling of these components with the antennas. Even with the 50% copper flux rings being added, the internal magnetic field strength does not drop significantly, indicating that these rings have not reduced RMF penetrability significantly and that any coupling between antennas is not resistive. And as expected, when the load is present it absorbs much of the energy of the system, shielding the internal magnetic probe.

Other general trends were seen throughout testing. To begin with, it was suspected that the aluminum flux rings would result in poorer internal magnetic field strength than copper rings of the same dimensions due to larger skin depth which would cause the RMF to be shielded and damped. The test results confirmed this hypothesis in all antenna cases. To illustrate this, Table 2 shows key results of testing five copper rings with 50% opacity and five aluminum rings with 50%

**Table 2. Comparison between copper and aluminum 5-50% flux rings for 1-turn Litz doubled and lapped antennas and 1-turn double solid copper antenna, both wired both in series and parallel.**

| Antenna Type | Wiring | Flux Ring Type | $Q_{avg}$ | $B_{R,norm}$ (G) |
|---|---|---|---|---|
| Doubled Litz | Parallel | Cu | 46±44% | 0.65 |
| | | Al | 34±36% | 0.66 |
| | Series | Cu | 57±1% | 0.75 |
| | | Al | 57±32% | 0.73 |
| Lapped Litz | Parallel | Cu | 48±36% | 0.72 |
| | | Al | 28±21% | 0.71 |
| | Series | Cu | 65±14% | 0.79 |
| | | Al | 56±1% | 0.77 |
| Doubled solid copper | Parallel | Cu | 31±37% | 0.59 |
| | | Al | 25±10% | 0.59 |
| | Series | Cu | 41±8% | 0.67 |
| | | Al | 33±12% | 0.67 |

opacity on the antennas: 1-turn doubled Litz connected in series and in parallel, 1-turn lapped Litz connected in series and in parallel and 1-turn doubled solid copper connected in series and in parallel. In each case the normalized magnetic field strength produced was very similar, but the Q factors in the aluminum cases were lower, meaning that energy was lost through higher resistive coupling.

**Table 3. Copper flux ring geometry comparison for the 1-turn doubled Litz antenna connected in series.**

| Copper Flux Rings | $Q_{avg}$ | $B_{Rnorm}$ (G) |
|---|---|---|
| none | 67±13% | 0.82 |
| five, 25% | 76±1% | 0.78 |
| five, 50% | 57±1% | 0.75 |
| five, 90% | 51±10% | 0.58 |
| 13, 25% | 58±1% | 0.76 |

Next, the 1-turn and 2-turn lapped Litz antennas were compared for various test cases with differing flux ring geometries and presence of dummy loads. The test capacitances were 1.98 and 0.66 µF, and the antenna inductances were 152 and 358 nH, respectively. For the cases with flux rings and no loads, the 2-turn antennas produced on average 25% more internal radial magnetic field than their 1-turn counterparts. Similarly, 2-turn circuit Qs were about 70% greater than the 1-turns. It was expected that the 2-turn antennas should produce fields about the same as the 1-turns, because energy in the circuit was held constant. Of course manufacturing 2-turn versions of the antennas is more difficult, particularly if using solid copper rather than Litz wire.

Next, the results for the 1-turn lapped Litz antenna wired in parallel and in series were compared. Results are shown in Table 4 as ratios of parallel to series. The series wiring resulted in higher circuit Q values when no load was present, but resulted in equal Q values when a load was present. The magnetic field magnitudes produced by series and parallel were comparable over all cases. Therefore, it appears that the series wiring is preferable.

**Table 4. Comparison of series and parallel wirings of the 1-turn lapped Litz antenna.**

| Test Case | $Q_{avg}$ parallel/ $Q_{avg}$ series | $B_{R,norm}$ parallel/ $B_{R,norm}$ series |
|---|---|---|
| OMF only | 0.56 | 0.91 |
| RMF only | 0.53 | 0.93 |
| RMF 5-25% Cu flux rings | 0.56 | 0.90 |
| RMF 5-25% Cu flux rings with load | 0.98 | 0.89 |
| RMF 13-25% Cu flux rings | 0.73 | 0.88 |
| RMF 13-25% Cu flux rings with load | 0.95 | 0.87 |
| RMF 5-50% Cu flux rings | 0.73 | 0.91 |
| RMF 5-50% Cu flux rings with load | 0.93 | 1.01 |

Next, the doubled Litz antenna and doubled solid copper antenna were compared for various test cases to determine how much the material affected the results. Similar to the comparison between the 1-turn and 2-turn antennas of the same geometry, presented are the solid copper antenna values for circuit Q and normalized magnetic energy, each divided by the Litz antenna values, as shown in Table 5. Across multiple cases the solid antenna performs only slightly worse than the Litz antenna at these frequencies. For this reason, it would be reasonable to construct future antennas out of either Litz wire or crushed solid copper tubing, depending on heating concerns or ease of construction desired, without sacrificing much in performance. It would be expected that Litz would have significantly more effect at higher frequencies, where skin depths are smaller.

The next trend to identify was which antenna material and geometry combination performed the best over the rest of the antennas in the same areas as in the above comparisons. Recall that the magnetic field strengths have been normalized and that discharge energy has been held roughly constant. The three antennas that stand out as performing better than all others through all iterations of flux ring geometries are in order: 2-turn lapped Litz in parallel, 1-turn lapped Litz in series, and the 1-turn lapped Litz in parallel. The data for these three antennas is shown in Table 6.

The same problems with inconsistencies in average circuit Q are present, again because of antenna coupling problems. Otherwise, the fact that all of the lapped antennas tested performed better than all other antennas implies that the lapped RF antenna geometry is superior to the doubled geometry in terms of maximum internal radial field and average circuit Q factor.

**Table 5. Comparison of Litz and solid copper doubled antennas wired in parallel.**

| Test Case | $Q_{avg}$ Solid/ $Q_{avg}$ Litz | $B_{R,norm}$ Solid/ $B_{R,norm}$ Litz |
|---|---|---|
| OMF only | 0.81 | 1.00 |
| RMF only | 0.74 | 0.93 |
| RMF with load | 0.82 | 0.91 |
| RMF 5-25% Cu flux rings | 0.82 | 0.91 |
| RMF 5-25% Cu flux rings with load | 0.96 | 0.93 |
| RMF 13-25% Cu flux rings | 0.71 | 0.95 |
| RMF 13-25% Cu flux rings with load | 0.95 | 0.97 |

Finally, the fully constructed version of the EMPT thruster, shown in Fig. 1, was also tested with the same measurement setup and assessment method. Its test parameters and resulting data are shown in Table 7. The thruster implements square, aluminum structural plates and a 2-turn doubled Litz RMF antenna. Comparing the values in Table 6 to those in Table 7, it is clear that the thruster did not perform well in comparison to many of the antenna-flux ring combinations tested over the course of this study. Having shown that aluminum flux rings are inferior to copper flux rings, the presence of the large aluminum plates is likely the major cause of this. Exchanging the doubled antenna for a lapped antenna would also likely improve performance.

**Table 6. Comparison of Best Performing Antennas.**

| Antenna | Cu Flux Rings | $Q_{avg}$ | $B_{R,norm}$ (G) |
|---|---|---|---|
| 2-turn lapped Litz in parallel | none | 63±24% | 0.99 |
| | 5, 25% | 58±1% | 0.95 |
| | 5, 50% | 47±1% | 0.88 |
| | 5, 90% | 51±11% | 0.67 |
| 1-turn lapped Litz in series | none | 62±24% | 0.82 |
| | 5, 25% | 61±24% | 0.82 |
| | 5, 50% | 65±14% | 0.79 |
| | 5, 90% | 50±11% | 0.60 |
| 1-turn lapped Litz in parallel | none | 33±4% | 0.76 |
| | 5, 25% | 35±26% | 0.74 |
| | 5, 50% | 48±35% | 0.72 |
| | 5, 90% | 32±5% | 0.54 |

**Table 7. Old EMPT thruster test parameters and results for the 2-turn doubled Litz RMF antenna.**

| | $Q_{avg}$ | $B_{R,norm}$ (G) | Frequency (kHz) | DC Voltage (V) | Capacitance (μF) |
|---|---|---|---|---|---|
| OMF | 37 | 0.50 | 298 | 710 | 1.98 |
| RMF | 35 | 0.47 | 300 | 700 | 1.98 |

## IV. Conclusion

This paper has documented the process by which the geometry and material of the RMF antennas and flux rings were optimized to reduce undesirable resistive coupling and increase plasma loading within the EMPT thruster. Multiple configurations were tested in air empty and with a stainless steel plasma simulation load. The resulting data indicates that copper flux rings shield the plasma from the RMF less than do aluminum rings of the same surface coverage and moreover, that five rings of 25% coverage maximized radial field strength. The lapped antenna geometry produced greater field strength than did the doubled geometry. Litz and solid copper antennas of the same geometry and number of loops performed similarly, meaning that ease of construction and heating are considerations which will guide the choice of one over the other. 2-turn antennas outperformed 1-turn antennas of the same geometry and the antenna identified as performing better than all others was the 2-turn lapped parallel-connected Litz antenna. Finally, when comparing the field strength and Q factor produced when using this antenna with that produced by the latest version of the EMPT thruster, Mark III Version 3, it was clear that its design should be altered to improve performance. Namely, the aluminum support plates should be removed, aluminum flux rings should be replaced with five 25% coverage copper rings, and the antenna geometry should be changed from the doubled configuration to the lapped. After this study was performed a redesigned EMPT, shown in Fig. 12, was constructed accordingly and has begun testing with a plasma load.

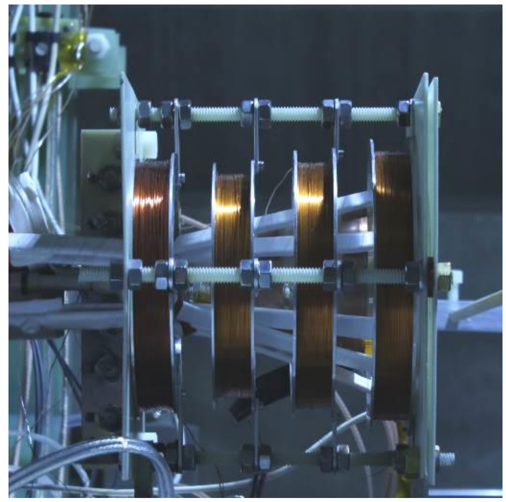

**Figure 12. Newly redesigned EMPT.**

## Appendix

**Table A. Inductances of antennas tested.**

| Antenna | Wiring | Antenna A Inductance (nH) | Antenna B Inductance (nH) | Capacitance (μF) | DC Avg. Voltage (V) | RMF Frequency (kHz) |
|---|---|---|---|---|---|---|
| 1-turn doubled Litz | Parallel | 130 | 120 | 1.98 | 430 | 275 |
| | Series | 510 | 460 | 0.66 | 690 | 262 |
| 1-turn lapped Litz | Parallel | 150 | 150 | 1.98 | 420 | 294 |
| | Series | 510 | 510 | 0.66 | 680 | 263 |
| 2-turn doubled Litz | Parallel | 360 | 340 | 0.66 | 710 | N/A |
| | Series | 1370 | 1290 | N/A | N/A | N/A |
| 2-turn lapped Litz | Parallel | 350 | 350 | 0.66 | 710 | 307 |
| | Series | 1410 | 1410 | N/A | N/A | N/A |
| 1-turn doubled solid copper | Parallel | 150 | 130 | 1.98 | 430 | 285 |
| | Series | 470 | 410 | 0.66 | 710 | 285 |
| Thruster 1-turn doubled | Series | 425 | 425 | 1.98 | 700 | 299 |

**Table B. Flux conserving ring geometries.**

| Ring Set | Material | Opacity (%) | Number of Rings | Thickness (mm) | Width (mm) |
|---|---|---|---|---|---|
| A | Aluminum | 50 | 5 | 1 | 8.2 |
| B | Copper | 50 | 5 | 0.8 | 8.2 |
| C | Copper | 90 | 5 | 0.8 | 14.8 |
| D | Copper | 25 | 5 | 0.8 | 4.1 |
| E | Copper | 25 | 13 | 0.8 | 2.1 |


## Acknowledgments

I would like to thank my supervisor Dr. David Kirtley for his enthusiasm, incredible depth of knowledge, and unending patience. I thank MSNW president Dr. John Slough and the entire team for their supporting efforts and their humor. And I thank Michael Pfaff for being my diligent editor and a dear friend.


## References


[1] Kirtley, D., Slough, J., Pfaff, M., Pihl, C., "**S**teady Operation of an Electromagnetic Plasmoid Thruster," *Joint Army Navy NASA Air force Conference*, 2011.

[2] Slough, J., Kirtley, D., Thomas, W., "Pulsed Plasmoid Propulsion: The ELF Thruster," *31st International Electric Propulsion Conference*, IEPC-2009-265, Ann Arbor, 2009.

[3] Kirtley, D., Pancotti, A., Slough, J., and Pihl, C. "Steady Operation of an FRC Thruster on Martian Atmosphere and Water Propellants," *Joint Propulsion Conference*, 2012.

[4] Tuszewski, M., "Field Reversed Configurations," *Nuclear Fusion* Vol. 28, 2033, 1988.

[5] Blevin, H.A., Thonemann, P.C., "Plasma Confinement using an Alternating Magnetic Field," *Nucl. Fus. Suppl*. Part I, 55, 1962.

[6] Jones, I.R., "A review of rotating magnetic current drive…," *Phys. of Plasmas*, Vol. 6, 1950, 1999.

[7] Hugrass, W.N., Grimm, R.C., "A numerical study of the generation of an azimuthal current in a plasma cylinder using a transverse rotating magnetic field," *J. Plasma Physics*, 26 455, 1981.